Published in final edited form as:

Nat Struct Mol Biol. 2017 August ; 24(8): 643–651. doi:10.1038/nsmb.3427.

Regulator-dependent mechanisms of C3b processing by factor I allow differentiation of immune responses

Xiaoguang Xue[1], **Jin Wu**[1], **Daniel Ricklin**[2,5], **Federico Forneris**[1,5], **Patrizia Di Crescenzio**[2], **Christoph Q Schmidt**[2,3], **Joke Granneman**[1], **Thomas H Sharp**[4], **John D Lambris**[2], and **Piet Gros**[1]

[1]Crystal and Structural Chemistry, Bijvoet Center for Biomolecular Research, Department of Chemistry, Faculty of Science, Utrecht University, Utrecht, the Netherlands [2]Department of Pathology & Laboratory Medicine, University of Pennsylvania, Philadelphia, Pennsylvania, USA [3]Institute of Pharmacology of Natural Products and Clinical Pharmacology, Ulm University, Ulm, Germany [4]Section Electron Microscopy, Department of Molecular Cell Biology, Leiden University Medical Center, Leiden, the Netherlands

Abstract

The complement system labels microbes and host debris for clearance. Degradation of surface-bound C3b is pivotal to direct immune responses and protect host cells. How the serine protease factor I (FI), assisted by regulators, cleaves either two or three distant peptide bonds in the CUB domain of C3b remains unclear. We present a crystal structure of C3b in complex with FI and regulator factor H (FH; domains1–4 with 19–20). FI binds C3b–FH between FH domains 2 and 3 and a reoriented C3b C-terminal domain and docks onto the first scissile bond, while stabilizing its catalytic domain for proteolytic activity. One cleavage in C3b does not affect its overall structure, whereas two cleavages unfold CUB and dislodge the thioester-containing domain (TED), affecting binding of regulators and thereby determining the number of cleavages. These data explain how FI generates late-stage opsonins iC3b or C3dg in a context-dependent manner, to react to foreign, danger or healthy self signals.

The mammalian complement system in blood and interstitial fluids provides protection against invading microbes and contributes to tissue maintenance[1,2]. Upon complement

Correspondence should be addressed to P.G. (p.gros@uu.nl).

[5]The Armenise–Harvard Laboratory of Structural Biology, Department of Biology and Biotechnology, University of Pavia, Pavia, Italy (F.F.); Department of Pharmaceutical Sciences, University of Basel, Basel, Switzerland (D.R.).

AUTHOR CONTRIBUTIONS

J.W. cloned human factor 1, MCP and CR1. D.R. and C.Q.S. cloned miniFH. X.X. and J.G. cloned DAF. X.X. and F.F. purified C3b. X.X. produced and purified human FI, DAF, MCP and CR1. C.Q.S. produced and purified miniFH. X.X. crystallized C3b-miniFH and C3b-miniFH-FI complexes, collected X-ray diffraction data, determined and refined the structures. X.X. and T.H.S. prepared negative-stain EM samples, collected and analyzed EM data. X.X. collected and analyzed small angle X-ray scattering data. D.R. and P.D.C. performed surface plasmon resonance experiments and analysis. J.D.L. and P.G. supervised the project. X.X. and P.G. performed data analysis and interpretation, and wrote the manuscript. All authors critically revised the manuscript.

COMPETING FINANCIAL INTERESTS

The authors declare no competing financial interest.

Note: Any Supplementary Information and Source Data files are available in the online version of the paper.

activation, surfaces of microbes, non-healthy host cells and debris are extensively marked (opsonized) by C3b molecules, either via pathways initiated by specific recognition of surface-danger patterns or through a low-level, nonspecific autonomous activation of complement[3–5]. Local overactivation of complement due to deposits, such as soft drusen and amyloid-β plaques, may induce bystander damage to neighboring cells, causing deterioration of vision in age-related macular degeneration (AMD)[6] and loss of long-term memory in Alzheimer's disease[7,8]. To avoid self-injury, complement activation is controlled. An important mechanism of protection is provided by FI. FI is recruited to sites of complement activation by so-called cofactors, which belong to a protein family of regulators of complement activity (RCA)[9]. FI binds to cofactor–C4b or cofactor–C3b complexes and subsequently degrades C4b and C3b by cleaving them up to two and three times, respectively, in their complement C1r/C1s, Uegf, Bmp1 (CUB) domains, yielding proteolytic fragments iC4b and iC3b (after one and two cleavages, respectively) or C4c/C4d and C3c/C3dg (after two and three cleavages, respectively). These fragments cannot form C3 and C5 convertases and thereby stop further opsonization and generation of membrane-attack complexes. Mutations in RCA proteins, FI, C3b and C4b have been linked to atypical hemolytic uremic syndrome (aHUS) and dense deposit disease (DDD), diseases of dysregulated complement control manifested in kidneys[10]. Moreover, the proteolytic fragments produced by FI cleavage induce cellular innate and adaptive immune responses that aid in clearance of opsonized material. Complement receptors CR3 and CR4 and CRIg on macrophages bind iC3b and/or C3dg, inducing phagocytosis of the labeled cell or particle[4,5,11]. Phagocytosis induced by the interaction between CR3 on microglia and iC3b on synaptic compartments is important for synaptic pruning, suggesting that complement may have a role in schizophrenia and multiple sclerosis[12]. Antigen-conjugated C3dg or iC3b enhance the immune response via interactions with the CR2 on follicular dendritic cells and B cells[13,14].

FI is a five-domain trypsin-like serine protease, consisting of an FI membrane-attack complex domain (FIM), a scavenger receptor cysteine-rich domain (SRCR), and two low-density lipoprotein receptor class A (LA1 and LA2) domains followed by a C-terminal catalytic serine protease (SP) domain[15]. FI is secreted as a mature disulfide-linked two-chain enzyme, consisting of a heavy chain (Lys19–Ile335, containing the FIM, SRCR, LA1 and LA2 domains) and a light chain (Ile340–Val583, forming the SP domain). However, in solution, free FI has extremely low activity toward its native substrates C3b and C4b[16]. A crystal structure determined at 2.7-Å resolution of FI purified from human plasma showed a highly disordered SP domain[15]. Similar to that of thrombin without interacting partners[17], the low enzyme activity of free FI has been attributed to disorder in its SP domain[15]. Mutagenesis and domain truncation data show that the FIM domain and the hydrophobic interface between FI's heavy and light chains are critical for FI activation[18], because the FI SP domain alone cannot cleave C3b or C4b efficiently, regardless of the presence of a cofactor[16]. Thus, to cleave C3b or C4b efficiently, FI requires its regulatory heavy chain and complement regulators that exert cofactor activity.

RCA proteins, or regulators, contain strings of consecutive complement-control-protein (CCP) domains. In humans, the RCA family includes fluid-phase factor H (FH), C4b-binding protein, cell-surface-bound CR1 (CD35), membrane cofactor protein (MCP or

CD46), and decay-accelerating factor (DAF or CD55)[9]. Apart from acting as a cofactor to FI (referred to as cofactor activity), these proteins may enhance dissociation of the C3-convertase enzyme complexes (called decay-acceleration activity). Structures of C3b in complex with three to four consecutive CCP domains from several regulators showed that the regulators share an extended binding platform on C3b[19,20]. Furthermore, the last two C-terminal domains of FH, CCP19 and CCP20, interact with the C3b TED and the host surface, mediating self-recognition and protection[21,22]. In addition to differences in C3b and C4b affinities, there are large variations in activities among the regulators. DAF exhibits only decay-acceleration activity and has no cofactor activity, whereas MCP has only cofactor activity, and FH and CR1 have both[9]. Furthermore, CR1 effectively supports three cleavages by FI, whereas FH supports high activity for the first two cleavages and very low activity for the third one, and MCP yields only two cleavages[23]. A vaccinia-virus-encoded homolog, vaccinia complement protein (VCP), shows high activity for one cleavage of C3b[24]. Smallpox inhibitor of complement (SPICE), encoded by variola virus, differs in only 11 residues from VCP and has markedly higher activity with respect to human C3b[25]. Thus, differences among regulators affect the proteolytic fragments produced by FI on the surfaces of opsonized particles and cells. However, how the cofactors aid FI in performing its proteolytic function and how the differences in regulators affect the number of cleavages by FI remains unclear.

Crystal structures of C3b and C4b show that the scissile bonds in the CUB domains are 20–26 Å apart[26,27]. The predominant sequence of cleavage in C3b is first Arg1303–Ser1304; second, Arg1320–Ser1321; and third, Arg954–Glu955 (ref. 28) (using UniProt numbering). A docking model based on the crystal structures of free FI and C3b in complex with FH domains CCP1–4 (ref. 19) positioned FI in a niche between the C-terminal C3b (CTC) domain and domains CCP1–3 of FH with the catalytic domain toward Arg1303–Ser1304 in the C3b CUB domain[15]. Domains CCP1–3 have been shown to be important for cofactor activity of FH[29,30], whereas domain swapping of DAF and MCP indicated that only CCP2 and CCP3 in MCP are involved in its cofactor activity[31]. The first two cleavages in C3b remove residues 1304–1320 (C3f fragment), disrupting the factor B (FB) binding site that is required for C3-convertase formation[32]. Furthermore, these two cleavages yield structural arrangements of a C3c-like core with a flexibly attached TED, indicating an unfolded and extended CUB domain[33,34]. In contrast, Alcorlo *et al.* reported a compact arrangement of iC3b with TED localized near the CTC domain[35]. Taking these results together, it is unclear whether consecutive cleavages depend on large rearrangements in C3b and iC3b and whether regulators and FI rearrange to establish productive enzyme-substrate complexes for the three scissile bonds.

Here we present a crystal structure of the complex formed by human C3b, a shortened variant of FH, and FI. The structure provides a structural basis for understanding cofactor activity and cleavage of C3b by FI. EM and small-angle X-ray scattering (SAXS) showed the structural effects upon one or two cleavages in C3b. Based on these data, together with binding and functional cleavage data, and structures of other C3b–regulator complexes[20], we propose a mechanistic model for cofactor-assisted sequential cleavages of C3b by FI. The model explains why MCP allows FI to cleave C3b only twice, FH two or three times

(depending on the reaction time) and CR1 three times, yielding different proteolytic fragments of C3b on the cell or particle surface inducing immune responses.

RESULTS

Crystal structures of C3b–miniFH and C3b–miniFH–FI

We crystallized human plasma-derived C3b, a short variant of human FH, or miniFH, consisting of CCP domains 1–4 and 19–20, connected by 12 glycine residues[36], and catalytically inactivated (S525A) human FI. Structures of C3b–miniFH and C3b–miniFH–FI at 4.2-Å resolution (Fig. 1) were determined by molecular replacement[37] using known structures of C3b–FH CCP1–4 (PDB 2WII)[19], C3d–FH CCP19–20 (PDB 3OXU)[21] and FI (PDB 2XRC)[15](Table 1 and Supplementary Fig. 1). In both C3b–miniFH and C3b–miniFH–FI, the polyglycine linker and part of CCP20 were not resolved in the density and were omitted from the models. The carboxyl and amino ends of CCP4 and CCP19, respectively, are 36–37 Å apart in the models, in agreement with the presence of a 12-residue linker (Supplementary Fig. 1c). MiniFH binds C3b identically to the binding of its separate components: CCP1–4 and CCP19–20 to C3b and C3d, respectively (Supplementary Fig. 1d)[21,22], with minimal contacts between CCP4 and CCP19. In C3b–miniFH–FI, density was present for the loops in the SP domain of FI that were missing in the 2.7-Å structure of free FI, even though the current resolution was limited to 4.2 Å. The model for SP was completed by building loops, residues 394–408, 471–485, 514–524 and 547–553, and its amino-terminal tail, residues 340–353 (Supplementary Fig. 1e).

CTC of C3b reorients upon FI binding to C3b–miniFH

C3b–miniFH maintains its conformation upon binding FI, except for a marked 34° rotation of the CTC domain of C3b (Fig. 1a–c). This orientation of CTC is established by a β-turn-β configuration of the ‘neck’ region (residues 1496–1514), placing CTC in an upward position[20], and a twisting of a hinge loop formed by residues 1515–1526 (Supplementary Fig. 1f). In contrast, in C3b complexes with FH CCP1–4 and MCP, the neck region adopts a helical configuration, positioning the CTC downward, whereas C3b–SPICE, C3b–CR1, C3b–DAF and C3b–miniFH (without FI) display the β-turn-β configuration and have CTC in the upward position[20]. However, only the C3b–miniFH–FI complex reveals an additional twist of the CTC domain required for FI binding. Therefore, an ‘open’ CTC–CUB–TED arrangement of C3b is needed for binding FI; thus, the ‘closed’ CTC–CUB–TED as observed in C3b–regulator complexes of FH CCP1–4 and MCP[20] is not relevant for FI binding.

FI interactions with C3b–miniFH

FI binds C3b–miniFH at three sites formed by (i) the CTC domain of C3b, (ii) the regulator FH, and (iii) the macroglobulin (MG) domain 2 and CUB domain of C3b (Fig. 1d). A total of ~2,560 $Å^2$ surface area is buried at these interfaces in C3b–miniFH–FI, with 780, 1,010 and 990 $Å^2$ for each site, respectively.

The rotation of the CTC domain of C3b facilitates interactions of the heavy chain of FI with the ‘back’ side of CTC (where the FH- binding site is defined as the front side).

Hydrophobic residues V1657, V1658 and F1659, and the methylene groups of the K1570 side chain from the C-terminal helix α2 and V1576 from loop β2–β3 of the C3 CTC domain[27], interact with a hydrophobic patch on FI formed by residues I55, V60, L63, P64, Y65, F82, P83 and L91 of the FIM domain (Fig. 2a). In addition, C3b CTC E1654, the carboxyl group of N1663 and E1575 make interactions with K69, R80 of FI FIM and R575 of FI SP, respectively (Fig. 2a). Furthermore, a charge interaction is observed between C3b CTC E1575 and FI SP R575 (Fig. 2a). Mutations K69A, R80A and L91A reduced FI activity for its natural substrate C3b[38], which confirms the arrangement observed in the crystal structure. The V1658A polymorphism of C3 has been linked to aHUS; though previously attributed to gain-of-function in FB binding to C3b[39], this mutation lies in the middle of the FI-binding site and is outside the FB-binding site on the CTC domain of C3b (Supplementary Fig. 2a,b). C3b V1658 contacts both P64 and P83 of FI, for which mutations P64L and P83Q have been linked to AMD and aHUS[40]. P64L possibly causes steric hindrance at the interface, whereas P83Q additionally introduces a hydrophilic moiety at the hydrophobic interface.

Only domains CCP2 and CCP3 of FH make contact with FI in C3b–miniFH–FI (Fig. 3a), with approximately 650 and 390 Å^2 buried surface area, respectively. FH CCP2 residues L121, I124, I138 and I140 form a large hydrophobic patch that facilitates van der Waals interactions with W393, P402, L404, I407, V408, I409 and Y411 of FI. A smaller hydrophobic patch, formed by FH residues L147, P148 and F197 of CCP3, interacts with FI residues I400, H401 and F482. Residues 394–408 were largely unstructured in free FI (Supplementary Fig. 1e)[15]. Putative hydrogen bond and charge interactions are observed for E123, N136, D137 and E142 of FH CCP2 with R406, K441, K437 and K358 of FI, respectively. The charge interaction of FH E123 and FI R406 likely contributes considerably to the stabilization of FI, because both residues have been linked to disease-related mutations[41,42], and R406 is part of the unstructured loop 394–408 in free FI[15]. Several other disease-related FH mutations map onto CCP2–3 and the neighboring region on CCP1, indicating either direct or indirect effects on the FI-binding interface (Supplementary Fig. 2d).

The most marked change between the structures of free FI and FI bound to C3b–miniFH is the enhanced ordering of the catalytic SP domain. The SP domain of FI is buttressed in C3b–miniFH–FI by interactions with FH CCP2–3, interactions with the C3b CTC domain transmitted by the heavy chain of FI and, additionally, three charge interactions between FI SP R383 and C3b CUB D973, FI SP R389 and C3b MG2 E197 (Fig. 2b) and FI SP R575 and C3b CTC E1575 (Fig. 2a). FI mutant R389H has been linked to AMD; this mutation abrogates the observed charge interaction between the FI SP domain and C3b MG2.

In C3b–miniFH–FI the five domains of the FI heavy chain rotate as a rigid body by 11° compared to free FI (Supplementary Fig. 3a). The heavy chain is connected to the light chain, or SP domain, by the C327-C453 disulfide bond and a hydrophobic patch consisting of Y38 and F47 of FIM and I285 of LA2 contacting W456, L460 and Y459 of SP (burying ~400 Å^2 interface area; Fig. 2c). Mutations F47A and I285A at this interface reduce FI activity for its natural substrates C3b and C4b[18]. Moreover, FI mutant W456L and Y459S in this interface have been linked to aHUS and AMD[43].

FI interactions with FH and the heavy chain resemble ligand binding at exosites 1 and 2 of thrombin[17]. FI loop 358–363 corresponds to the thrombin 37s loop (Supplementary Fig. 3b,c) and contains K358, which interacts with E142 of FH (Fig. 3). Furthermore, FI loop 394–408 corresponds to the thrombin 70s loop and becomes ordered upon interactions with FH CCP2–3. Together, the 37s and 70s loops correspond to exosite 1 in FI. The relatively short FI loop 471–485 relates to the γ loop in thrombin and provides F482 for hydrophobic contacts (Fig. 3 and Supplementary Fig. 3b,c). Thus, interactions with miniFH CCP2–3 at FI's exosite 1 and interactions of C3b CTC with FI's heavy chain, transmitted through the heavy chain–light chain interface, stabilize the SP domain.

First scissile bond of C3b docked into active center of FI

The active site of FI in the C3b–miniFH–FI crystal structure is consistent with an active configuration of the catalytic triad H380, D429 and S525 (without its nucleophilic hydroxyl moiety due to the S525A mutation) and the terminal NH_2 group of I340 in place to stabilize the oxyanion hole (Fig. 3b). Density is present for the N-terminal tail of the FI SP domain, residues 340–353, in contrast to a disordered loop observed in the structure of free FI[15]. R1303 of C3b CUB binds FI D519 of the S1-binding pocket and the first scissile bond R1303-S1304 docks into the FI catalytic center (Fig. 3b). The scissile loop 1300–1306 of C3b is flipped out with respect to other structures of C3b (Supplementary Fig. 4a). The first and third scissile loops of C3b have relatively high *B* factors in C3b crystal structures (which are not observed for the second scissile loop), indicating a higher local flexibility that facilitates a rearrangement to dock into the active site of FI (Supplementary Fig. 4b).

FI–regulator interactions for cofactor activity

Structure-based sequence alignment of cofactors shows that CR1 CCP16–17 and MCP CCP2–3 each have hydrophobic patches for FI binding to their CCPii and CCPiii domains (using generic numbering of CCP domains according to FH numbering)[20](Supplementary Fig. 5a). FH residue E142, at the C-terminal end of the CCP2 domain, is positioned between these two hydrophobic patches and makes a charge interaction with FI K358 (Fig. 3a). A negatively charged residue at this position is conserved in MCP, whereas CR1 CCP9 and CCP16 have glutamine at this position. In contrast, DAF does not have these hydrophobic patches on its CCP3 and CCP4 domains (corresponding to CCPii and CCPiii). DAF E187, which corresponds to FH I140, disrupts the hydrophobic patch in CCP3 and E243 disrupts the patch in CCP4 (Supplementary Fig. 5b). In addition, R189 at the C-terminal end of DAF CCP3 abolishes a possible charge interaction with FI K358. Moreover, DAF differs from cofactors not only because of the absence of the hydrophobic patches required for FI binding. Superposition of regulator–C3b complexes[19], superposed on CCPii–iii domains to highlight local differences, shows that DAF yields a different relative orientation of the C3b CUB that is not compatible with the hypothetical position of the FI SP domain for catalysis.

The distribution of charged residues around the FI-binding site in CCP2 differs for FH when compared to MCP CCP2 and CR1 CCP9 and CCP16. FH E123 is in a unique position to interact with FI R406 (in loop 394–408) because it has a one-residue insert compared to other cofactors, yielding a bulge in the main chain conformation (Fig. 3a; Supplementary Fig. 6). This negative charge is absent in the CR1 cofactor regions. Although MCP has two

glutamate residues in the sequence at this site, both residues point away from FI R406. Furthermore, FH D137 interacts with K437 of FI. However, both CR1 CCP16 and MCP have a lysine at this position (Supplementary Fig. 6a). Similarly, modification of E120K from VCP to SPICE is responsible for 32-fold increase in activity[25]. These data on charge interactions appear to be in conflict with the arrangement observed in the C3b–miniFH–FI crystal structure, which represents the situation for cofactors with a negative charge at this position. Compared to FH, the other cofactors have four more residues between Cys129 and Cys141 (Supplementary Fig. 6a). The opposing area in FI is formed by residues 435–448. This amino acid stretch is rich in charged residues (^{435}xKKDxxKKDxExxR^{448}) and exhibits relatively high *B* factors (Supplementary Fig. 6b). Possibly, residues 435–448 of FI adjust their conformation and adapt to the pattern of charges present on the various cofactors. Besides E120K, mutations H98Y and S103Y account for the increase in activity going from VCP to SPICE[25] (Supplementary Fig. 6c). Residue 98 participates in hydrophobic interactions between FH and FI; replacing a histidine in VCP by a tyrosine in SPICE potentially increases hydrophobic interactions and thereby increases activity. However, the effect from serine-to-tyrosine modification at position 103 remains unclear, because residue 103 is not located at the FH-FI interface. Thus, these data indicate that the heavily charged peptide stretch loop 435–448 in FI possibly adjusts to accommodate charge variations present in different regulators.

Overall shape unaffected by one cleavage in C3b

We used VCP to generate C3b that is cleaved predominantly once by FI[24], referred to as iC3b1. iC3b1 was prepared by incubating C3b with FI and VCP for 1 h at 37 °C; iC3b was obtained by incubating C3b with FI and miniFH for 10 min at 37 °C (Online Methods; Supplementary Fig. 7a,b). The purified C3b, iC3b1 and iC3b were used for negative-stain EM and small-angle X-ray scattering (SAXS). Averaging and 2D classification of individual particles extracted from EM images showed that the overall shape of iC3b1 was for the majority of classes similar to that of C3b (gray averages, Fig. 4a; Supplementary Fig. 7c), indicating that noncovalent interactions are maintained to keep CUB TED associated with the main body of C3b and iC3b1, irrespective of cleavage at the first site. 2D classification of iC3b (or iC3b2), however, resulted in classes indicating dislocation of TED and unfolding of CUB (Fig. 4a, red and blue averages), similar to previous observations[33] and contradicting a previous report by another group[35]. SAXS of C3b, iC3b1 and iC3b confirmed the EM analysis (Fig. 4b; whereas scattering- intensity curves from C3b and iC3b1 are similar, iC3b differs from C3b and iC3b1. C3b, iC3b1 and iC3b exhibit radii of gyration of 48, 48 and 53 Å and longest dimensions of 164, 166 and 200 Å, respectively. *Ab initio* reconstructions yielded similar shapes for C3b and iC3b1 and an elongated shape for iC3b (Supplementary Fig. 7d).

Relative affinities of regulator fragments for C3b, iC3b and C3c

CR1 supports three rapid cleavages, whereas FH supports two cleavages efficiently and the third cleavage only in low-ionic-strength environment or prolonged incubation; MCP aids FI to cleave C3b only twice (Supplementary Fig. 8a)[23,24,44]. Using surface plasmon resonance (SPR), we analyzed the relative binding activities of regulator fragments for C3b, iC3b and C3c (Fig. 5; Supplementary Fig. 8b). In agreement with earlier reports[19], FH fragment

CCP1–4 binds C3b more strongly than FH CCP1–3. FH CCP1–3 binds with comparable, yet very weak, affinity to C3b, iC3b and C3c, suggesting that this interaction does not depend on the CUB and TED domains. The low binding profile of FH CCP1–4 for iC3b and C3c is comparable to that observed for FH CCP1–3. Thus, CUB unfolding and TED dislocation in iC3b, and the absence of CUB–TED in C3c, explains the reduced affinity of FH CCP1–4 for iC3b and C3c. The higher affinity of FH CCP1–4 for C3b requires interactions with folded CUB and TED placed next to MG1 (ref. 19). A similar dependence of properly folded and bound CUB–TED can be claimed in the case of MCP, because no binding to iC3b or C3c could be detected for this regulator. Although less residual binding to iC3b and C3c was observed for MCP when compared to FH CCP1–4, the concentration range use does not enable a quantitative assessment (Supplementary Fig. 8b). Finally, the binding data for CR1 CCP15–17 shows that this fragment strongly binds to C3b but with some ten-fold weaker affinity to iC3b and C3c (Fig. 5; Supplementary Fig. 8b). These relative interaction profiles are consistent with the observed cofactor activities. CR1 binds relatively strongly to C3b and iC3b, thereby supporting three cleavages. In contrast, MCP binds only to C3b but not to iC3b, thus supporting two cleavages. FH binds C3b, supporting two cleavages. Overall, the efficiency of cofactor activity depends on the binding affinity, which decreases from miniFH, through FH CCP1–4 to FH CCP1–3 (ref. 19). At prolonged incubation times, however, FH apparently overcomes the weak apparent binding to iC3b, showing that the interaction of CCP1–3 with the core of C3b and iC3b suffices to yield three cleavages by FI under certain conditions.

DISCUSSION

Degradation of C3b by cofactor-assisted FI cleavage is critical for protection of host cells from complement attack and for processing of opsonized microbes and apoptotic host cells to invoke cellular responses[45]. The presented crystal structures reveal how the human regulator FH assists in binding FI to the C3b–FH complex and how the complex activates FI to cleave C3b at its first cleavage site. FI binds C3b–FH primarily at the CTC domain of C3b and domains CCP2–3 of FH. As predicted[15], the partially disordered SP domain of free FI is stabilized in the ternary C3b–FH–FI complex, indicating that its catalytic activity is induced similarly to thrombin activation by ligand binding[17]. FH domains CCP2 and CCP3 induce structure in loops 394–408 and 471–485 of the SP domain through critical hydrophobic regulator-FI interaction sites[31]. Surrounding charge interactions appear to be variable for different cofactor regulators. These variations are likely accommodated by conformational rearrangements of the highly charged residue stretch 435–448 in FI. Although DAF is structurally similar to other regulators, it lacks cofactor activity. Consistent with published DAF chimera data[31], DAF CCP3–4 does not contain the hydrophobic patches and critical charges for FI interactions, and in C3b–DAF, the CUB position differs from those of the cofactors (Supplementary Fig. 5c). C3b interacts primarily through its CTC domain with the FIM domain in the heavy chain of FI. Upon binding, the heavy chain reorients by 11° without significant conformational changes in the heavy chain or heavy and light chain interface. Nevertheless, a large number of mutations linked to AMD and aHUS[43], as well as effects from several experimental alanine mutations[18], indicate that the CTC-FIM interface, the integrity of the heavy chain and the heavy and light chain interface, are critical for

activity (Supplementary Note, Supplementary Table 1, and Supplementary Fig. 9). Overall, these data indicate that all interactions between C3b–FH and FI contribute, either directly or indirectly, to stabilization of the catalytic SP domain of FI and hence induce proteolytic activity to the enzyme.

The EM and SAXS analyses of the sequential substrate states, C3b, iC3b1 and iC3b, indicate that one cleavage does not affect the overall domain arrangement, whereas two cleavages unfolds CUB and dislodges TED. Here, we consider a simple mechanistic model in which the substrate putatively rearranges to facilitate sequential cleavage of the three distant scissile bonds in C3b CUB. The presented crystal structure revealed a composite arrangement needed to stabilize the catalytic domain of FI for proteolysis of the first bond, Arg1303-Ser1304. Cleavage of the first bond putatively induces local flexibility, allowing the subsequent stretch of amino acids (from residue 1,304 to ~1,323) to rearrange and position the second scissile bond Arg1320-Ser1321 into the active site. Unfolding of the CUB domain after the second cleavage yields an extended and flexible peptide chain between MG7 and TED (residues 935–985), which facilitates docking of the third bond, Arg954-Glu955, into the catalytic site for cleavage. In such a simple ‘substrate-readjustment’ model the FI SP domain remains buttressed by the C3b, or iC3b, CTC domain and cofactor CCPii–iii domains to induce catalytic activity (as observed in C3b–FH–FI). An alternative mechanism that would depend on different compact arrangements that stabilize and activate FI, either through concerted domain movements or rebinding, is difficult to conceive. Thus, the simplest model that agrees with our data implies that the substrate rearranges upon sequential cleavages with no or minor movements of the catalytic protease domain.

The proposed mechanistic ‘substrate-readjustment’ model for sequential cleavages of C3b provides an explanation for the difference in the number of cleavages supported by cofactor activities of CR1, FH and MCP. C3b provides a continuous binding platform for regulator domains CCPi–iv formed by the α′-chain N-terminal region, MG7, MG6, MG3, MG2, CUB, MG1 and TED[20]. After unfolding of CUB and dislodging of TED, as in iC3b, these two domains can no longer participate in cofactor binding. Our relative binding data show that CR1 CCP15–17 binds equally strong to C3c and iC3b; this is consistent with the crystal structure of C3b CR1 CCP15–17, which shows that these domains bind to the C3b CCPi–iii binding sites on the MG ring[20]. Correspondingly, CR1 cleaves C3b efficiently three times, because binding of CR1 barely depends on CUB or TED. In contrast, MCP cleaves C3b only twice. MCP binds C3b strongly and does not bind C3c or iC3b. As indicated by the crystal structure of C3b–MCP[20], MCP binding to C3b requires TED located next to MG1. Since TED-MG1 interactions are intact in C3b and iC3b1, MCP binds these two states and exerts its cofactor activity for cleaving sites one and two. Because TED is dislodged in iC3b, MCP loses its affinity and, therefore, does not support further cleavage of iC3b. Similar to MCP, FH cleaves C3b twice under physiological conditions, at which FH binds to C3b via binding sites CCPii–iv with TED being positioned next to the MG core[19]. At prolonged incubation times, however, FH supports three cleavages; the very weak binding of FH CCP1–3 to iC3b (similar to the C3c interaction) appears to be sufficient for enabling FI to cleave the third site over time. Thus, the cofactor-binding affinity for the CCP-binding site on the C3c-like core of C3b and the dependence on additional affinity provided by binding

to TED determines the number of cleavages and, hence, the production of either iC3b or C3dg and C3c, by FI.

Overall, our data provide insights into the underlying mechanisms of host-cell protection and differential processing of C3-opsonized microbes and apoptotic host cells to invoke cellular responses (Fig. 6). When C3b binds inadvertently to healthy host cells, such as in situations that may lead to bystander damage, host regulators like cell-surface bound MCP bind C3b, which facilitates binding and activation of FI to cleave C3b. Cleavages of C3b at Arg1303-Ser1304 and Arg1320-Ser1321 disrupt the CUB-binding site required for factor B binding in the formation of C3 convertases[32,46], thereby stopping the amplification loop of complement activation. However, on cells that either lack or have insufficient protective regulators, such as invading microbes and apoptotic host cells, amplification by C3 convertases leads to rapid opsonization with C3b. The exposure of a C3b-opsonized cell to a distinct set of complement regulators, whether present on the cell surface, recruited from plasma or mediated by another cell, largely defines the fate of this cell and the immune response that is raised. For example, reduced expression of MCP and CR1 (ref. 47) and the enhanced recruitment of FH to apoptotic cell surfaces[48] indicate that processing of opsonized apoptotic host cells involves mostly FH; the two FI cleavages mediated by this regulator yield an iC3b opsonin that stimulates phagocytosis by immature dendritic cells[49], thereby preventing excessive complement activation and inflammation[50,51]. Heavily opsonized microbial cells may face a diverse set of regulator-mediated actions depending on their environment, including lysis and inflammation, clearance by phagocytosis and/or the adherence to erythrocytes with shuttling to the spleen followed by processing by and transfer between follicular dendritic cell and B cells in the lymph nodes to help in raising an adaptive immune response[52,53]. Thus, the molecular mechanism of cofactor-assisted sequential proteolysis of C3b by FI, as deduced from the presented structural data, is governed by the C3b-binding patterns of the regulators and provides the basis for the differential processing and immune recognition of opsonized material from different sources.

ONLINE METHODS

Protein purification

Human FI mutated at S525A was co-expressed with furin in N-acetylglucoaminyltransferase I-deficient human embryonic kidney 293 cells that stably express Epstein-Barr virus nuclear antigen I (HEK293-ES, supplied by U-Protein Express BV (U-PE), Utrecht, the Netherlands). Expression yielded FI cleaved at 336–339, consistent with the mature state of the enzyme. Secreted matured FI was captured by incubating culture medium with Ni-excel beads (GE Healthcare) at room temperature for 1 h, followed by a washing step using 25 mM HEPES pH 7.5, 500 mM NaCl, 15 mM imidazole. After elution using the same buffer supplemented with 250 mM imidazole, the sample was subjected to a gel-filtration step using a Superdex 200 10/300 GL (GE Healthcare) equilibrated in 25 mM HEPES pH 7.5 and 100 mM NaCl. Additional proteolysis was observed in purified FI samples after prolonged storage at room temperature and 4 °C (Supplementary Fig. 10). This second proteolytic event was attributed to cleavage at ^{315}RRR^{317}.

MiniFH consisting of human FH CCP1–4 and CCP19–20 connected by a polyglycine linker was expressed in *Pichia pastoris* and purified according to previous work[36].

Human CR1 CCP15–17, MCP CCP1–4, FH CCP1–4 and FH CCP1–3 were expressed in HEK293-ES cells[20]. Recombinant VCP was expressed and purified from *P. pastoris* as previously described[24].

Human C3b was obtained by treating C3 purified from healthy donors with recombinant FB and factor D, as described[32]. The nascent thioester was blocked by iodoacetamide to prevent dimerization of C3b.

iC3b1 was generated by incubating C3b with FI and VCP in a molar ratio 1:0.001:1 at 37 °C for 1 h. The digestion mixture was loaded onto monoQ 5/50 GL (GE Healthcare) column, followed by a gradient washing step. Fractions containing iC3b1 were collected and purified by gel-filtration column (Superdex 200 10/300 GL, GE Healthcare). iC3b, or iC3b2, was produced by incubating C3b with FI and miniFH in molar ration 1:0.001:1 at 37 °C for 1 h and purified by gel-filtration column (Superdex 200 10/300 GL, GE Healthcare).

Crystallization, data collection and structure determination

Crystals of C3b–miniFH–FI were grown in 60 mM sodium malonate pH 5.0, 6% w/v PEG3350, using the hanging drop vapor diffusion method at 18 °C. Crystals were soaked for several minutes in reservoir solution supplemented with 25% v/v glycerol and then flash frozen in liquid nitrogen. Diffraction data were collected at European Synchrotron Radiation Facility (ESRF) and Swiss Light Source at Paul Scherrer Institute (SLS-PSI). Diffraction data were processed by XDS[54] and AIMLESS[55]. Crystals of C3b–miniFH–FI exhibited space group $P1$ and diffracted to a resolution of 3.8 Å. However, the diffraction data was highly anisotropic. The data were therefore truncated to 4.2-Å resolution and rescaled using the Diffraction Anisotropy Server[56]. The structure was determined by molecular replacement with Phaser[37], using known structures of C3b–FH CCP1–4 (PDB 2WII[19]), C3d–FH CCP19–20 (PDB 3OXU[21]) and FI (PDB 2XRC[15]). Crystals of C3b–minFH–FI contained two copies of the complex in the $P1$ unit cell. The structure was refined by Phenix[57]. Because the resolution of ternary complex structure was low, we used the structure of C3b (PDB 5FO7)[20], C3bFH (PDB 2WII)[58], and FI (PDB 2XRC)[15] as reference models in refinement. To improve the model quality, we further used PDB-redo[58] server to optimize our model. The model was finally refined yielding R / R_{free} values of 23.0% / 25.4%, with acceptable stereochemistry. The quality of the refined electron density map is presented in Supplementary Figure 1.

C3b–miniFH complex crystals were grown in 60 mM ammonium sulfate, 6% w/v PEG3350, using the hanging drop vapor diffusion method at 18 °C. Crystals were soaked for several minutes in reservoir solution supplemented with 25% glycerol (v/v) and then flash frozen in liquid nitrogen. Diffraction data were collected at the ESRF and SLS. Data were processed by XDS[54] and AIMLESS[55]. Crystals exhibited space group $P3_121$ and diffracted to a resolution of 4.2 Å. The structure was determined by molecular replacement using Phaser[37]. The data were affected by merohedral twinning, as determined by *phenix.xtriage*[57]. Thus, in order to refine the structure properly, the twin-law operator -h,-k,l was used as twin-

refinement target in *phenix.refine*[57]. The final model was refined to R / R_{free} values of 21.6% / 24.6%, with good stereochemistry. Data collection and refinement statistics are summarized in Table 1.

Negative-stain electron microscopy

Purified C3b, iC3b1, and iC3b were loaded onto glow-discharged carbon-coated copper grids and stained with 0.75% uranyl formate. Grids were imaged using a Tecnai T20 transmission electron microscope (Thermo Fisher Scientific) operating at 120 kV with an objective lens spherical aberration coefficient of 2 mm. Images were acquired at 56000× magnification with a defocus of –2 μm on a Gatan Ultrascan 4k charged coupled device (Gatan, Inc.) binned 2× for a final pixel size of 4.236 Å per pixel. Image data was processed by EMAN2 (ref. 59) and Xmipp[60] as previously described[61]. Briefly, 6,927, 5,997, 8,022 particles were manually picked for C3b, iC3b1 and iC3b, respectively, using e2boxer.py from EMAN2 (ref. 59), and extracted using Xmipp[60]. The CTF of each micrograph was estimated and corrected by phase flipping using Xmipp. Finally, each data set was classified into 30 classes by CL2D protocol in Xmipp[60].

Small-angle X-ray scattering

Purified C3b, iC3b1 and iC3b were prepared in 25 mM HEPES pH 7.5 and 100 mM NaCl. SAXS data were collected at the ESRF beamline BM29 on a Pilatus 2M detector (Dectris) using the standard setup for size-exclusion chromatography coupled SAXS mode[62]. A Superdex 200 column (GE Healthcare) connected to an HPLC system (Shimadzu) was used for size-exclusion chromatography to separate aggregates from monodisperse samples. Raw data were preprocessed by DATASW[63], and frames showing radiation damage were removed before analysis. The *ab initio* shapes of all the samples were modeled based on buffer-subtracted data by DAMMIF from ATSAS suite[64]. All SAXS curves were compared and plotted by SAXSview (http://saxsview.sourceforge.net).

Surface plasmon resonance

Interaction analysis between opsonins and the various regulators was performed on a Biacore 3000 instrument (GE Healthcare) at 25 °C using PBS pH 7.4 containing 0.005% Tween-20 as running buffer. C3b, iC3b and C3c (all from Complement Tech) were immobilized on separate flow cells of a CM5 sensor chip using standard amine coupling. The immobilization densities were adjusted under consideration of each protein's molecular weight to provide a comparable number of binding sites (6,100–7,600 RU). A non-modified flow cell was used for signal referencing. Injections with the complement inhibitor compstatin (analog 4(1MeW)), which binds to the C3c part common in all tested opsonins, were used to validate the activity of each surface. Subsequently, linear concentration series of FH CCP1–3, FH CCP1–4, MCP and CR1 (20 μM–10 nM) were simultaneously injected onto all flow cells at 20 μl/min with injection contact times of 1 min; all injection signals returned to baseline levels without the need for surface regeneration. All data were processed using Scrubber (v2.0c; BioLogic Pty, Australia). Steady-state responses were fit to a single binding site model and normalized to the calculated maximum binding response (R_{max}) to reflect the binding signals as percentage of the binding capacity.

Cofactor assays

Cofactor assays were performed in PBS buffer using the same method as previously described[25]. Briefly, purified C3b (~1 μg) incubated with regulators and FI in a molar ratio of 1:1:0.001 in a total volume of 6 μl at 37 °C. The reaction was stopped by adding SDS-PAGE loading buffer with DTT. The cleavage results were analyzed by SDS-PAGE.

Structural models and sequence alignments

All structural figures were generated using Pymol[65]. Structure-based sequence alignment was performed by T-coffee and 3D T-coffee[66].

Data Availability

Coordinates and structure factors for C3b-miniFH-FI and C3b-miniFH have been deposited in the Protein Data Bank with accession codes PDB 5O32 and PDB 5O35. Other data available from the corresponding author upon reasonable request.

Supplementary Material

Refer to Web version on PubMed Central for supplementary material.

Acknowledgments

We gratefully thank the European Synchrotron Radiation Facility (ESRF) and the Swiss Light Source (SLS) for the provision of synchrotron radiation facilities and beamline scientists of the ESRF, SLS and the European Molecular Biology Laboratory for assistance. We gratefully acknowledge P. Afanasyev and R. Koning for discussion and assistance in EM data collection and analysis. The work was financially supported by a Top grant (700.54.304 to P.G.) by the Council for Chemical Sciences of the Netherlands Organization for Scientific Research (NWO-CW), the European Research Council (grant no. 233229), the European Community's Seventh Framework Programmes (FP7/2007-2013) under BioStruct-X (grant no. 283570) and FP7/DIREKT (grant no. 602699 to J.D.L.), and grants by the US National Institutes of Health (AI068730, AI030040; to J.D.L.) and National Science Foundation (no. 1423304 to D.R.). P.G. was further supported by the Institute for Chemical Immunology, an NWO Gravitation project funded by the Ministry of Education, Culture and Science of the Netherlands.

References

1. Ricklin D, Hajishengallis G, Yang K, Lambris JD. Complement: a key system for immune surveillance and homeostasis. Nat Immunol. 2010; 11:785–797. [PubMed: 20720586]
2. Stephan AH, Barres BA, Stevens B. The complement system: an unexpected role in synaptic pruning during development and disease. Annu Rev Neurosci. 2012; 35:369–389. [PubMed: 22715882]
3. Walport MJ. Complement. First of two parts. N Engl J Med. 2001; 344:1058–1066. [PubMed: 11287977]
4. Merle NS, Church SE, Fremeaux-Bacchi V, Roumenina LT. Complement system part I—molecular mechanisms of activation and regulation. Front Immunol. 2015; 6:262. [PubMed: 26082779]
5. Merle NS, Noe R, Halbwachs-Mecarelli L, Fremeaux-Bacchi V, Roumenina LT. Complement system part II: role in immunity. Front Immunol. 2015; 6:257. [PubMed: 26074922]
6. Zipfel, PF., Lauer, N., Skerka, C. Inflammation and Retinal Disease: Complement Biology and Pathology. Lambris, JD., Adamis, AP., editors. Vol. 703. Springer; New York: 2010. p. 9-24.
7. Lambert JC, et al. Genome-wide association study identifies variants at CLU and CR1 associated with Alzheimer's disease. Nat Genet. 2009; 41:1094–1099. [PubMed: 19734903]
8. Brouwers N, et al. Alzheimer risk associated with a copy number variation in the complement receptor 1 increasing C3b/C4b binding sites. Mol Psychiatry. 2012; 17:223–233. [PubMed: 21403675]

9. Zipfel PF, Skerka C. Complement regulators and inhibitory proteins. Nat Rev Immunol. 2009; 9:729–740. [PubMed: 19730437]
10. Ricklin D, Reis ES, Lambris JD. Complement in disease: a defence system turning offensive. Nat Rev Nephrol. 2016; 12:383–401. [PubMed: 27211870]
11. Lin Z, et al. Complement C3dg-mediated erythrophagocytosis: implications for paroxysmal nocturnal hemoglobinuria. Blood. 2015; 126:891–894. [PubMed: 26082452]
12. Ramaglia V, et al. C3-dependent mechanism of microglial priming relevant to multiple sclerosis. Proc Natl Acad Sci USA. 2012; 109:965–970. [PubMed: 22219359]
13. Carroll MC. The complement system in regulation of adaptive immunity. Nat Immunol. 2004; 5:981–986. [PubMed: 15454921]
14. Kemper C, Atkinson JP. T-cell regulation: with complements from innate immunity. Nat Rev Immunol. 2007; 7:9–18. [PubMed: 17170757]
15. Roversi P, et al. Structural basis for complement factor I control and its disease-associated sequence polymorphisms. Proc Natl Acad Sci USA. 2011; 108:12839–12844. [PubMed: 21768352]
16. Tsiftsoglou SA, et al. The catalytically active serine protease domain of human complement factor I. Biochemistry. 2005; 44:6239–6249. [PubMed: 15835912]
17. Lechtenberg BC, Johnson DJD, Freund SMV, Huntington JA. NMR resonance assignments of thrombin reveal the conformational and dynamic effects of ligation. Proc Natl Acad Sci USA. 2010; 107:14087–14092. [PubMed: 20660315]
18. Nilsson SC, et al. Analysis of binding sites on complement factor I that are required for its activity. J Biol Chem. 2010; 285:6235–6245. [PubMed: 20044478]
19. Wu J, et al. Structure of complement fragment C3b-factor H and implications for host protection by complement regulators. Nat Immunol. 2009; 10:728–733. [PubMed: 19503104]
20. Forneris F, et al. Regulators of complement activity mediate inhibitory mechanisms through a common C3b-binding mode. EMBO J. 2016; 35:1133–1149. [PubMed: 27013439]
21. Morgan HP, et al. Structural basis for engagement by complement factor H of C3b on a self surface. Nat Struct Mol Biol. 2011; 18:463–470. [PubMed: 21317894]
22. Kajander T, et al. Dual interaction of factor H with C3d and glycosaminoglycans in host-nonhost discrimination by complement. Proc Natl Acad Sci USA. 2011; 108:2897–2902. [PubMed: 21285368]
23. Lambris JD, et al. Dissection of CR1, factor H, membrane cofactor protein, and factor B binding and functional sites in the third complement component. J Immunol. 1996; 156:4821–4832. [PubMed: 8648130]
24. Sahu A, Isaacs SN, Soulika AM, Lambris JD. Interaction of vaccinia virus complement control protein with human complement proteins: factor I-mediated degradation of C3b to iC3b1 inactivates the alternative complement pathway. J Immunol. 1998; 160:5596–5604. [PubMed: 9605165]
25. Yadav VN, Pyaram K, Mullick J, Sahu A. Identification of hot spots in the variola virus complement inhibitor (SPICE) for human complement regulation. J Virol. 2008; 82:3283–3294. [PubMed: 18216095]
26. Mortensen S, et al. Structural basis for the function of complement component C4 within the classical and lectin pathways of complement. J Immunol. 2015; 194:5488–5496. [PubMed: 25911760]
27. Janssen BJC, Christodoulidou A, McCarthy A, Lambris JD, Gros P. Structure of C3b reveals conformational changes that underlie complement activity. Nature. 2006; 444:213–216. [PubMed: 17051160]
28. Ross GD, et al. Generation of three different fragments of bound C3 with purified factor I or serum. II Location of binding sites in the C3 fragments for factors B and H, complement receptors, and bovine conglutinin. J Exp Med. 1983; 158:334–352. [PubMed: 6224880]
29. Hocking HG, et al. Structure of the N-terminal region of complement factor H and conformational implications of disease-linked sequence variations. J Biol Chem. 2008; 283:9475–9487. [PubMed: 18252712]

30. Pechtl IC, Kavanagh D, McIntosh N, Harris CL, Barlow PN. Disease-associated N-terminal complement factor H mutations perturb cofactor and decay-accelerating activities. J Biol Chem. 2011; 286:11082–11090. [PubMed: 21270465]
31. Gautam AK, et al. Mutational analysis of Kaposica reveals that bridging of MG2 and CUB domains of target protein is crucial for the cofactor activity of RCA proteins. Proc Natl Acad Sci USA. 2015; 112:12794–12799. [PubMed: 26420870]
32. Forneris F, et al. Structures of C3b in complex with factors B and D give insight into complement convertase formation. Science. 2010; 330:1816–1820. [PubMed: 21205667]
33. Nishida N, Walz T, Springer TA. Structural transitions of complement component C3 and its activation products. Proc Natl Acad Sci USA. 2006; 103:19737–19742. [PubMed: 17172439]
34. Papanastasiou M, et al. Structural implications for the formation and function of the complement effector protein iC3b. J Immunol. 2017; 198:3326–3335. [PubMed: 28258193]
35. Alcorlo M, et al. Unique structure of iC3b resolved at a resolution of 24 Å by 3D-electron microscopy. Proc Natl Acad Sci USA. 2011; 108:13236–13240. [PubMed: 21788512]
36. Schmidt CQ, et al. Rational engineering of a minimized immune inhibitor with unique triple-targeting properties. J Immunol. 2013; 190:5712–5721. [PubMed: 23616575]
37. McCoy AJ, et al. Phaser crystallographic software. J Appl Crystallogr. 2007; 40:658–674. [PubMed: 19461840]
38. Nilsson SC, et al. Analysis of binding sites on complement factor I that are required for its activity. J Biol Chem. 2010; 285:6235–6245. [PubMed: 20044478]
39. Sartz L, et al. A novel C3 mutation causing increased formation of the C3 convertase in familial atypical hemolytic uremic syndrome. J Immunol. 2012; 188:2030–2037. [PubMed: 22250080]
40. Rodriguez E, Rallapalli PM, Osborne AJ, Perkins SJ. New functional and structural insights from updated mutational databases for complement factor H, Factor I, membrane cofactor protein and C3. Biosci Rep. 2014; 34:635–649.
41. Dragon-Durey MA, et al. Heterozygous and homozygous factor h deficiencies associated with hemolytic uremic syndrome or membranoproliferative glomerulonephritis: report and genetic analysis of 16 cases. J Am Soc Nephrol. 2004; 15:787–795. [PubMed: 14978182]
42. Moore I, et al. Association of factor H autoantibodies with deletions of CFHR1, CFHR3, CFHR4, and with mutations in CFH, CFI, CD46, and C3 in patients with atypical hemolytic uremic syndrome. Blood. 2010; 115:379–387. [PubMed: 19861685]
43. Kavanagh D, Goodship TH, Richards A. Atypical hemolytic uremic syndrome. Semin Nephrol. 2013; 33:508–530. [PubMed: 24161037]
44. Ahmad M, et al. Domain swapping reveals complement control protein modules critical for imparting cofactor and decay-accelerating activities in vaccinia virus complement control protein. J Immunol. 2010; 185:6128–6137. [PubMed: 20956343]
45. Ricklin D, Reis ES, Mastellos DC, Gros P, Lambris JD. Complement component C3—The “Swiss Army Knife” of innate immunity and host defense. Immunol Rev. 2016; 274:33–58. [PubMed: 27782325]
46. Janssen BJC, et al. Insights into complement convertase formation based on the structure of the factor B-cobra venom factor complex. EMBO J. 2009; 28:2469–2478. [PubMed: 19574954]
47. Hart SP, Ross JA, Ross K, Haslett C, Dransfield I. Molecular characterization of the surface of apoptotic neutrophils: implications for functional downregulation and recognition by phagocytes. Cell Death Differ. 2000; 7:493–503. [PubMed: 10800083]
48. Gershov D, Kim S, Brot N, Elkon KB. C-Reactive protein binds to apoptotic cells, protects the cells from assembly of the terminal complement components, and sustains an antiinflammatory innate immune response: implications for systemic autoimmunity. J Exp Med. 2000; 192:1353–1364. [PubMed: 11067883]
49. Verbovetski I, et al. Opsonization of apoptotic cells by autologous iC3b facilitates clearance by immature dendritic cells, down-regulates DR and CD86, and up-regulates CC chemokine receptor 7. J Exp Med. 2002; 196:1553–1561. [PubMed: 12486098]
50. Trouw LA, et al. C4b-binding protein and factor H compensate for the loss of membrane-bound complement inhibitors to protect apoptotic cells against excessive complement attack. J Biol Chem. 2007; 282:28540–28548. [PubMed: 17699521]

51. Kang YH, Urban BC, Sim RB, Kishore U. Human complement Factor H modulates C1q-mediated phagocytosis of apoptotic cells. Immunobiology. 2012; 217:455–464. [PubMed: 22088229]
52. Verschoor A, et al. A platelet-mediated system for shuttling blood-borne bacteria to CD8α+ dendritic cells depends on glycoprotein GPIb and complement C3. Nat Immunol. 2011; 12:1194–1201. [PubMed: 22037602]
53. Broadley SP, et al. Dual-track clearance of circulating bacteria balances rapid restoration of blood sterility with induction of adaptive immunity. Cell Host Microbe. 2016; 20:36–48. [PubMed: 27345696]
54. Kabsch W. XDS. Acta Crystallogr D Biol Crystallogr. 2010; 66:125–132. [PubMed: 20124692]
55. Evans PR, Murshudov GN. How good are my data and what is the resolution? Acta Crystallogr D Biol Crystallogr. 2013; 69:1204–1214. [PubMed: 23793146]
56. Strong M, et al. Toward the structural genomics of complexes: crystal structure of a PE/PPE protein complex from *Mycobacterium tuberculosis*. Proc Natl Acad Sci USA. 2006; 103:8060–8065. [PubMed: 16690741]
57. Adams PD, et al. PHENIX: a comprehensive Python-based system for macromolecular structure solution. Acta Crystallogr D Biol Crystallogr. 2010; 66:213–221. [PubMed: 20124702]
58. Joosten RP, Long F, Murshudov GN, Perrakis A. The PDB_REDO server for macromolecular structure model optimization. IUCrJ. 2014; 1:213–220.
59. Tang G, et al. EMAN2: an extensible image processing suite for electron microscopy. J Struct Biol. 2007; 157:38–46. [PubMed: 16859925]
60. de la Rosa-Trevín JM, et al. Xmipp 3.0: an improved software suite for image processing in electron microscopy. J Struct Biol. 2013; 184:321–328. [PubMed: 24075951]
61. Scheres SHW, Núñez-Ramírez R, Sorzano COS, Carazo JM, Marabini R. Image processing for electron microscopy single-particle analysis using XMIPP. Nat Protoc. 2008; 3:977–990. [PubMed: 18536645]
62. Hutin S, Brennich M, Maillot B, Round A. Online ion-exchange chromatography for small-angle X-ray scattering. Acta Crystallographica D Structural Biology. 2016; 72:1090–1099. [PubMed: 27710930]
63. Shkumatov AV, Strelkov SV. DATASW, a tool for HPLC-SAXS data analysis. Acta Crystallogr D Biol Crystallogr. 2015; 71:1347–1350. [PubMed: 26057674]
64. Petoukhov MV, et al. New developments in the ATSAS program package for small-angle scattering data analysis. J Appl Crystallogr. 2012; 45:342–350. [PubMed: 25484842]
65. The PyMOL Molecular Graphics System, V 1.8. Schrödinger, LLC; 2015.
66. Notredame C, Higgins DG, Heringa J. T-Coffee: A novel method for fast and accurate multiple sequence alignment. J Mol Biol. 2000; 302:205–217. [PubMed: 10964570]

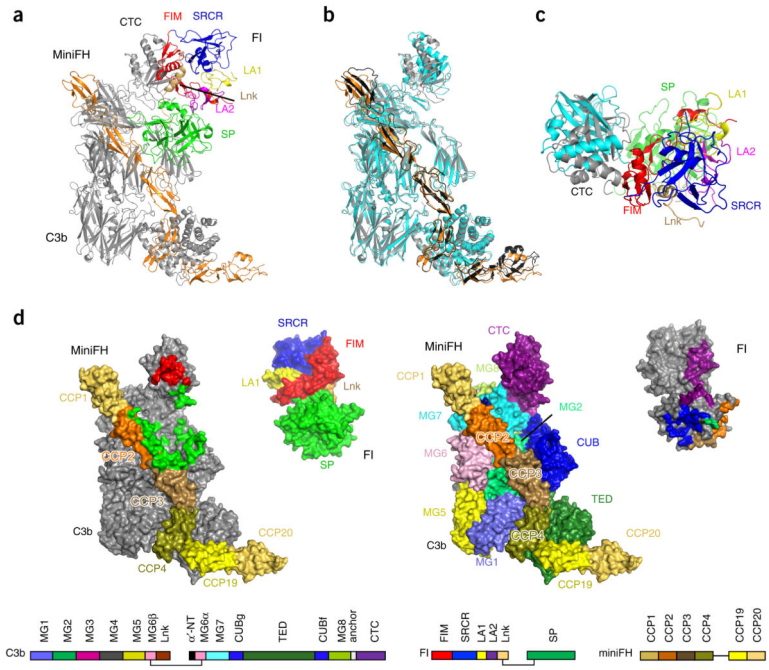

Figure 1.

Crystal structures of C3b–miniFH and C3b–miniFH–FI. (**a**) Structure of C3b–miniFH-FI. C3b, gray; miniFH, orange; FI colored by domain as shown at the bottom of the figure. (**b**) Superposition of C3b–miniFH (C3b, cyan; miniFH, black) and the corresponding parts from the C3b–miniFH–FI complex (C3b, gray; miniFH, orange). (**c**) Top view of superposition showing binding of FI (colored by domain as indicated) to CTC domain of C3b (gray); the CTC domain as found in C3b–miniFH is shown (cyan) for reference. (**d**) Contact regions for FI domains shown as footprints on C3b–miniFH (left) and contact region of C3b–miniFH domains on FI (right); domain coloring as defined by labels and schematic domain compositions of C3b, FI and miniFH as shown at the bottom.

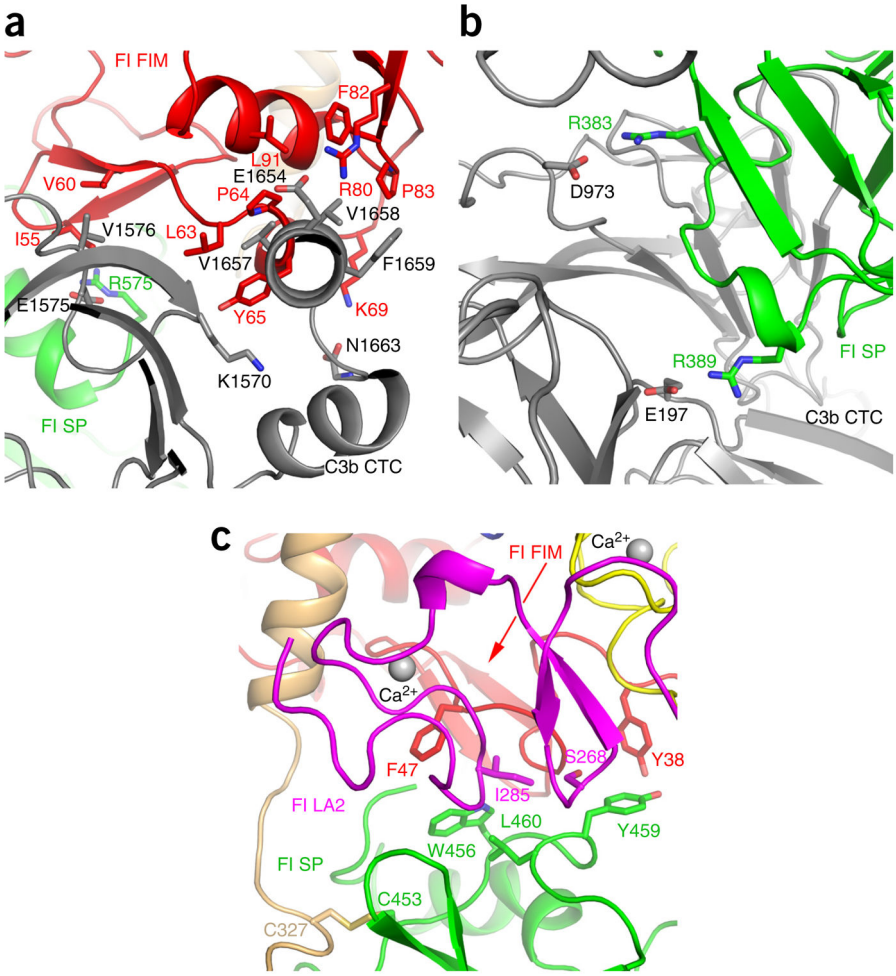

Figure 2.

Interactions of C3b–FI heavy chain and FI heavy-light chain in the C3b–miniFH–FI complex. (**a**) Hydrophobic contacts and two charge interactions between C3b CTC domain and FI FIM domain are shown. (**b**) Outside of the C3b cleavage sites, FI SP interacts with C3b domains MG2 and CUB through two charge interactions. (**c**) Interactions between FI heavy chain domains LA2 and FIM with FI SP. Color scheme as defined in Figure 1.

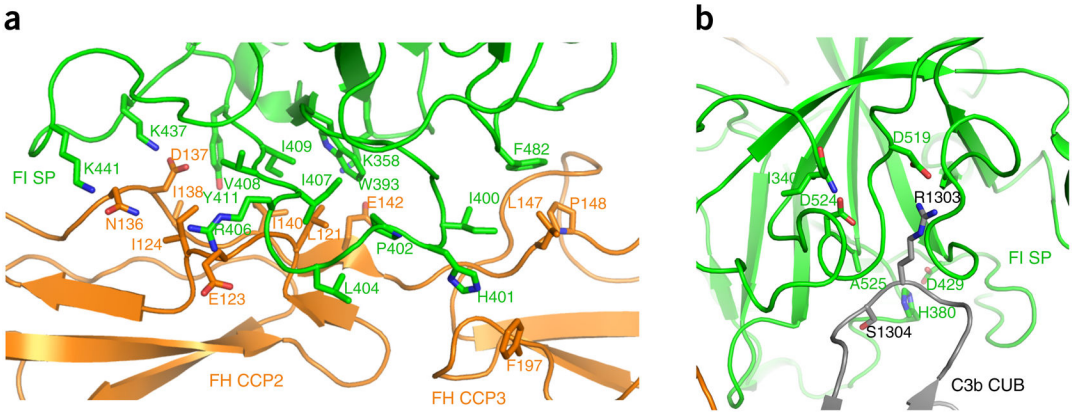

Figure 3.

Interactions of FI SP domain with FH CCP2-3 and C3b CUB. (**a**) FH CCP2 and CCP3 and FI SP are shown with interacting residues shown in sticks. (**b**) FI SP domain binds first scissile loop in C3b CUB domain in its active site. Shown are the scissile loop with cleavage site at R1303 and S1304 of C3b CUB, with R1303 bound to D519 of FI SP; the catalytic center of FI SP with D429, H380 and A525 (serine in wild-type FI) and I340 of the N-terminal tail of SP stabilizing the oxyanion hole. Color scheme as defined in Figure 1.

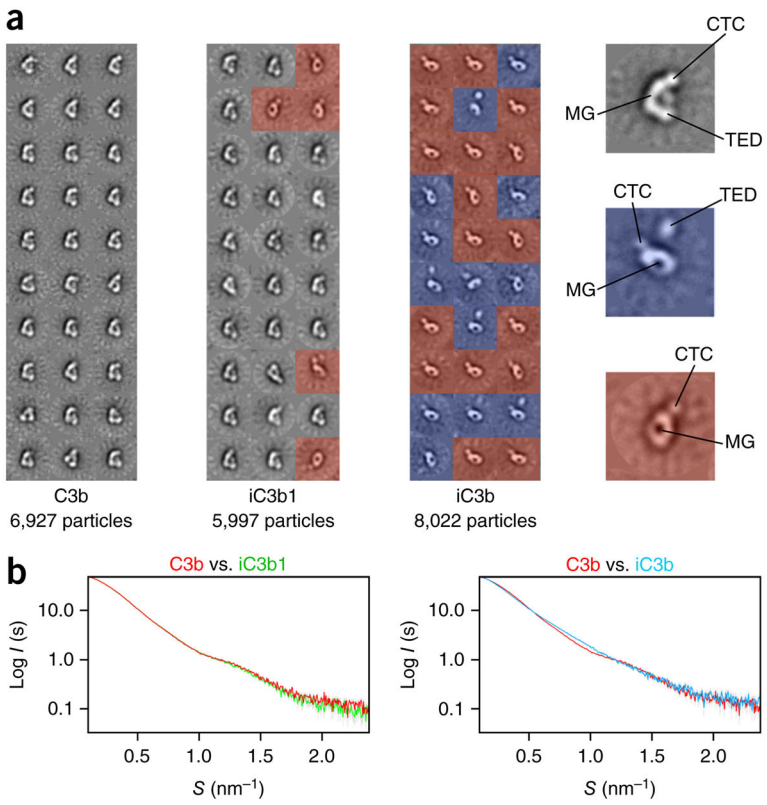

Figure 4.

iC3b1 resembles C3b, whereas iC3b exhibits a flexible and elongated CUB-TED. (**a**) Averaged and classified 2D particles for C3b, iC3b1 and C3b obtained by negative-stain EM, left, middle, and right, respectively. 2D averages with an overall shape corresponding C3b, gray; particles without an identifiable TED domain, red; particles with a dislodged TED domain, blue. (**b**) SAXS curves data of C3b (red) versus iC3b1 (green), left, and C3b (red) versus iC3b (blue), supporting the notion that the overall arrangement of domains in iC3b resembles C3b and that both differ from iC3b, which is characterized by a dislodged TED domain due to unfolding of the CUB domain.

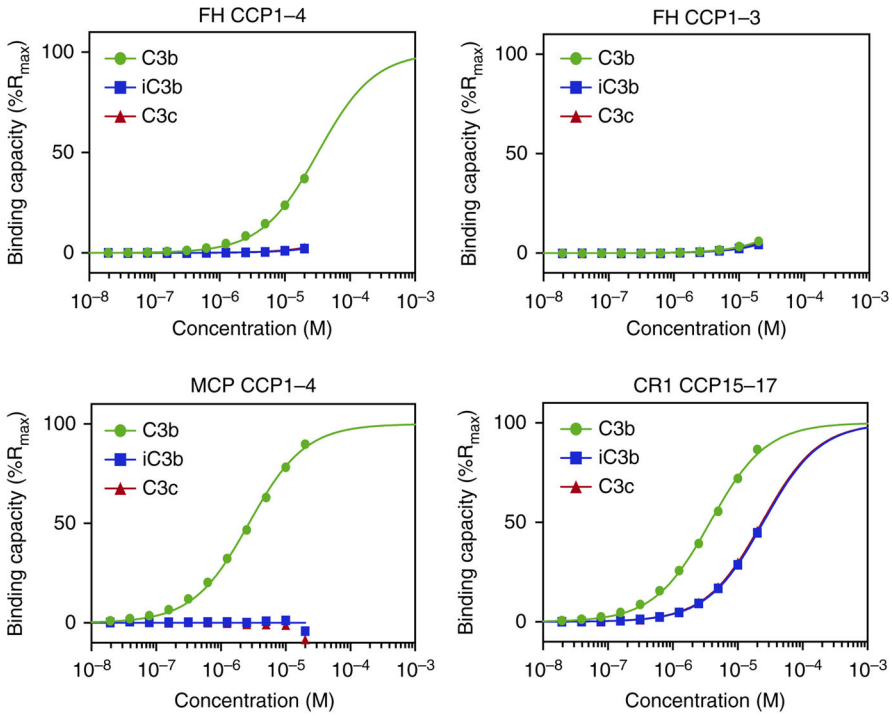

Figure 5.

Relative binding of regulator constructs to C3-derived fragments. SPR-derived binding data of regulator fragments FH CCP1–4, FH CCP1–3, MCP CCP1–4 and CR1 CCP15–17 toward C3b, iC3b and C3c. FH CCP1–4, MCP and CR1 CCP15–17 all show significant binding to C3b, whereas FH CCP1–3 binds much more weakly to C3b. In contrast, only CR1 CCP15–17 shows considerable interaction with iC3b and C3c; the apparent binding of FH CCP1–4, FH CCP1–3 and MCP is either very weak or not detectable under the conditions used for this study. Individual SPR sensorgrams and additional information about the interaction analysis are provided in Supplementary Figure 8b.

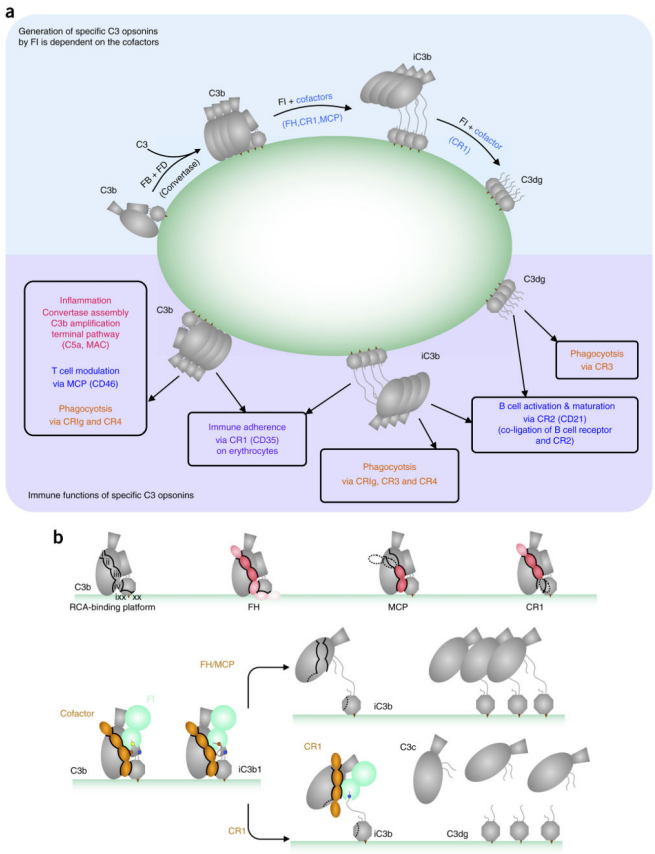

Figure 6.

Model of the molecular basis of cofactor activity. (**a**) Overview of regulator-dependent C3b proteolysis by FI in protection against over activation of the complement cascade and signaling adaptive immune responses. (**b**) RCA proteins, or regulators, share a common binding platform on C3b for binding; however, regulators differ in subsites exploited for binding. For instance, FH binds C3b mainly through CCP1–4 and CCP19–20 binding at binding sites i–iv, ixx and xx. MCP interacts with C3b MGs through CCP3–4 binding at sites iii–iv, whereas its other CCP domains do not contact C3b. CR1 (CCP15–17) mainly interacts with C3b through domains CCP16 and CCP17 binding at ii–iii. Curved black lines on C3b outline the common regulator-binding platform on C3b. The intensity of the red coloring of CCP domains reflects the relative contribution to binding affinity. (**c**) Regulators with cofactor activity bind C3b forming C3b-regulator complexes providing a binding platform for FI. Upon binding, FI is stabilized by interactions with the C3b-CTC domain and CCP domains of the regulator, which induces proteolytic activity, yielding cleavage of the first scissile bond (yellow) in the CUB domain of C3b. Cleavage of the first site (Arg1303-Ser1304, yellow) causes local flexibility in the CUB domain that exposes the second site (Arg1320-Ser1321, red), which is adjacent in sequence, for subsequent cleavage. After cleavage of these first two bonds, the CUB domain of the product iC3b becomes highly flexible and unfolds. Upon unfolding of the CUB domain, the TED domain becomes dislodged, thereby iC3b loses the CCP-binding site iv (dashed line). Cofactors that depend on the CCP-iv binding site for sufficient binding affinity, like MCP and FH, therefore only

produce iC3b fragments. In contrast, CR1 and its CCP15–17 fragment do not rely on interaction at site iv, and, therefore, the regulator remains bound, allowing FI to process iC3b further (for example, to cleave the third site, Arg954-Glu955, blue), yielding the final fragments C3dg and C3c.

Table 1

Data collection and refinement statistics.

	C3b–miniFH–FI (S525A) (PDB 5O32)	C3b–miniFH (PDB 5O35)
Data collection		
Space group	*P*1	$P3_121$
Cell dimensions		
a, *b*, *c* (Å)	116.4, 122.8, 157.2	142.9, 142.9, 312.7
α, *β*, *γ* (°)	69.8, 76.1, 70.1	90.0, 90.0, 120.0
Resolution (Å)	48.8–4.2 (4.4–4.2)[a]	61.9–4.2 (4.4–4.2)
R_{merge}	0.17 (0.63)	0.089 (0.343)
$I / \sigma (I)$	6.2 (2.4)	7.4 (2.3)
$CC_{1/2}$	0.98 (0.84)	0.99 (0.56)
Completeness (%)	93.1 (100.0)	99.9 (99.9)
Redundancy	3.5 (3.5)	2.0 (2.0)
Refinement		
Resolution (Å)	48.8–4.2 (4.4–4.2)	61.9–4.2 (4.4–4.2)
No. reflections	192,679 (19,373)	27,693 (2,689)
R_{work} / R_{free}	0.230 / 0.254	0.216 / 0.246
No. atoms		
Protein	38,732	15,153
Carbohydrate	352	26
Calcium	6	2
Malonate	1	0
Water	0	0
B factors (Å^2)		
Protein	107.9	143.0
Ligand/ion	143.5	191.7
R.m.s. deviations		
Bond lengths (Å)	0.004	0.002
Bond angles (°)	0.98	0.48

[a]Values in parentheses are for highest-resolution shell.